Level Set Segmentation using Statistical Shape Priors

Anonymous CVPR submission

Paper ID 193

Abstract

A novel and robust 3-D segmentation approach is proposed using level sets based on shape constraints. The approach depends on both the gray level and shape information. A partial differential equation (PDE) is developed to control the evolution of the level sets. The PDE does not include weighting coefficients to be tuned, overcoming the disadvantages of other PDE approaches. The shape information is gathered from a set of the signed distance maps representing the training data as a histogram of the occurrences of the points inside and outside the object. We use a novel statistical approach to get a probability density function (pdf) for the signed distance map of the points inside and outside and also the distribution of gray level inside and outside the object. The proposed statistical approach is based on modelling the empirical density function (normalized histogram of occurrence) for either the gray level distribution or signed distance map with a linear combination of Gaussians (LCG) with positive and negative components. We modify an Expectation-Maximization (EM) algorithm to deal with the LCGs and also propose a novel EM-based sequential technique to get a close initial LCG approximation for the modified EM algorithm to start with. The pdf's of the signed distance and intensity gray level are embedded in the speed function of the level set specifying the direction of evolution. Experimental results show how the approach is accurate in segmenting different types of 2-D and 3-D data sets including medical images.

1. Introduction

Surgical planning, navigation, medical visualization and diagnostics all benefit from image segmentation; and level sets segmentation has retained its attention (see [1, 2, 3, 4, 5, 6, 7]) due to their topological flexibility and independence of the parameterizations of the evolving contour. However, segmentation process is still a challenge because of the image noise and inhomogeneities; therefore segmentation algorithms can not depend only on image information but also have to exploit the prior knowledge of shapes and other properties of the structures to be segmented.

The incorporation of shapes and deformable models became popular with Leventon *et al.*[8, 9] and Shen *et al.* [10] by attracting the level set function to the likely shapes from a training set specified by principal component analysis (PCA). Recently, the approach of [8] was extended in [11, 12] and [13]. In [11], shapes are represented with a linear combination of 2D distance maps where the weight estimates maximize the distance between the mean gray values inside and outside the shape. In [12], the idea is to use a deterministic model to represent the desired shape as a linear combination of the weighted signed 2D distance maps, the weights being estimated by minimizing a mutual information based cost function. However, as noted in [11], the space of distance maps is not closed with respect to linear operations, so that the distance map for zero level shape of a linear combination of the maps does not necessarily coincide with the latter combination. As a result, the model may produce an unpredictable shape.

The training shapes are represented with the like linear combination of the training signed 2D distance maps also in the papers of a second research group [13]. Here, all the shapes are described with a multidimensional Gaussian probability model of the weights in the linear combination. But apart from a probabilistic description, the model has similar inconsistencies.

In [14], registration is combined with the segmentation process in an energy minimization problem. The evolving curve/surface is embedded in a higher dimensional level set function and registered iteratively with a shape model. In [15], a 3D shape-segmentation approach is proposed where a shape model is built from a set of training shapes using distance functions. A level set function evolves minimizing the shape alignment energy and the intensity gray level.

In this paper, a novel and robust segmentation approach is proposed based on the level set technique with shape constraints. The segmentation approach depends on both gray level intensity and shape information; whereas the shape information is gathered from a set of training shapes. A signed distance function is assigned to each shape and the signed distance values are collected in the form of a histogram representing the occurrences of each value. Probability density functions of the object and background are formed based on the signed distance value in addition to the gray level intensity. These functions are estimated using our new approach known as the modified expectation maximization (EM) which estimates the density function by a linear combination of Gaus-

sians (LCG) with positive and negative components. The estimated pdf's are used in a variational approach making the segmentation accurate and fast.

2. Shape Modelling by Level Sets

Shape representation is the main task in shape analysis. The selection of such representation is very important in several computer vision and medical applications such as registration and segmentation. There are several ways described in [8, 16, 17]. Although some of these ways are powerful enough to capture local deformations, they require a large number of parameters to deal with important shape deformations. So an emerging way to represent shapes is derived using level sets [18]. This representation is invariant to translation and rotation. Given a curve/surface V that represents boundaries of a certain shape, we can define the following level set function:

$$\phi(x,y,z) = \begin{cases} 0, & (x,y,z) \in V \\ d((x,y,z),V) & (x,y,z) \in R_V \\ -d((x,y,z),V) & \text{Otherwise} \end{cases} \quad (1)$$

where R_V is the region defined by the shape and $d((x,y,z),V)$ is the minimum Euclidean distance between the image location (x,y,z) and the curve/surface V.

Such representation can account for local deformations that are not visible for iso-contours that are far away from the original shape, and for geometrical features of the shape that can also be derived naturally from this representation.

By this representation, we can construct a database of curves/surfaces and signed distance functions that represent variations for a certain shape. So, given a set of aligned curves/surfaces $V_1, ..., V_N$, level sets $\phi_1, ..., \phi_N$ are calculated as training data. From this information, we can extract a histogram of the occurrences of signed distance values which characterizes the shape and its local variations. Also, a mean curve/surface V_M is calculated as an average of the corresponding points of all the training curves/surfaces. Simply, we can get this curve/surface by picking each point in the first training curve/surface and get the nearest points in the other curves/surfaces, then calculate the average as follows:

$$V_M(x_j,y_j,z_j) = \frac{1}{N}\sum_{i=1}^{N} V_i(x_i,y_i,z_i), \quad (2)$$

where (x_i,y_i,z_i) are the corresponding points.

3. Curve/Surface Evolution and Level Sets

Within the level set formalism [19, 20], the evolving curve/surface is a propagating front embedded as the zero level of a scalar function $\phi(x,y,z,t)$. The continuous change of $\phi(x,y,z,t)$ can be described by the partial differential equation:

$$\frac{\partial\phi(x,y,z,t)}{\partial t} + F(x,y,z)|\nabla\phi(x,y,z,t)| = 0, \quad (3)$$

where $F(x,y,z)$ is a velocity function and $\nabla = [\frac{\partial}{\partial x}, \frac{\partial}{\partial y}, \frac{\partial}{\partial z}]^T$. The function $\phi(x,y,z,t)$ deforms iteratively according to $F(x,y,z)$, and the position of the 2D/3D front is given at each iteration by solving the equation $\phi(x,y,z,t) = 0$. Practically, instead of Eq.(3), the value $\phi(x,y,z,t_{n+1})$ at step $n+1$ is computed from $\phi(x,y,z,t_n)$ at step n by the relation:

$$\phi(x,y,z,t_{n+1}) = \phi(x,y,z,t_n) - \triangle t \cdot F|\nabla\phi(x,y,z,t_n)|. \quad (4)$$

The design of the velocity function $F(x,y,z)$ plays the major role in the evolutionary process. Among several formulations proposed in [21, 22], we have chosen the following formulation:

$$F(x,y,z) = \nu - \epsilon k(x,y,z), \quad (5)$$

where $\nu = 1$ or -1 for the contracting or expanding front respectively, ϵ is a smoothing coefficient which is always small with respect to 1, and $k(x,y,z)$ is the local curvature of the front. The latter parameter acts as a regularization term.

4. Statistical Model for Density Estimation

In this paper we introduce a new algorithm called a modified Expectation-Maximization algorithm that approximates an empirical probability density function of scalar data with a linear combination of Gaussians (LCG) with positive and negative components. Due to both positive and negative components, the LCG approximates inter-class transitions more accurately than a conventional mixture of only positive Gaussians.

This approach is suitable for estimating the marginal density for either the gray level distribution $p_g(q)$ or signed distances $p_s(d)$ in each region in the given image. In the following section we will describe this model for estimating the marginal density for the gray level distribution $p_g(q)$ in each region and the similar way can be used to estimate the density of the signed distances $p_s(d)$ in the given image.

To identify the model accurately, we approximate the marginal gray level probability density in each region with a LCG having $C_{\mathrm{p},i}$ positive and $C_{\mathrm{n},i}$ negative components:

$$p_g(q|i) = \sum_{r=1}^{C_{\mathrm{p},i}} w_{\mathrm{p},i,r}\varphi(q|\theta_{\mathrm{p},i,r}) - \sum_{l=1}^{C_{\mathrm{n},i}} w_{\mathrm{n},i,l}\varphi(q|\theta_{\mathrm{n},i,l}); \quad (6)$$

such that $\int_{-\infty}^{\infty} p_g(q|i)dq = 1$. Here, q is the gray level, and $\varphi(q|\theta)$ is a Gaussian density having a shorthand notation $\theta = (\mu,\sigma^2)$ for its mean, μ, and variance, σ^2. In contrast to more conventional normal mixture models, the components are now both positive and negative and have only one obvious restriction in line with Eq. (6): $\sum_{r=1}^{C_{\mathrm{p},i}} w_{\mathrm{p},i,r} - \sum_{l=1}^{C_{\mathrm{n},i}} w_{\mathrm{n},i,l} = 1$. These weights are not the prior probabilities, and the LCG of Eq. (6) is considered as a functional form of the approximation of a probability density depending on parameters (w,θ) of each component.

The mixture of K LCGs, $p(q) = \sum_{i=1}^{K} w_i p(q|i)$, has the same form but a larger number of components, e.g., $C_{\rm p} = \sum_{i=1}^{K} C_{{\rm p},i}$ and $C_{\rm n} = \sum_{i=1}^{K} C_{{\rm n},i}$ if all the values $\theta_{{\rm p},i,r}$ and $\theta_{{\rm n},i,l}$ differ for the individual models:

$$p_g(q) = \sum_{r=1}^{C_{\rm p}} w_{{\rm p},r}\varphi(q|\theta_{{\rm p},r}) - \sum_{l=1}^{C_{\rm n}} w_{{\rm n},l}\varphi(q|\theta_{{\rm n},l}) \qquad (7)$$

To identify this model in the unsupervised mode, the mixed empirical distribution of gray levels over the image has to be first represented by a joint LCG of Eq. (7) and then partitioned into individual LCG-models for each class $i = 1, \ldots, K$.

Under the fixed number of the positive and negative components, C, the model parameters $\mathbf{w} = \{w_c; c = 1, \ldots, C\}$ and $\mathbf{\Theta} = \{\theta_c : c = 1, \ldots, C\}$ maximizing the image likelihood can be found using an EM algorithm introduced in Section 4.1. It modifies the conventional EM-scheme to take account of the components with alternating signs.

The modified EM algorithm is sensitive to both its initial state specified by the numbers of positive and negative Gaussians, and the initial parameters (mean and variance) of each component. To find a close initial LCG-approximation of the empirical distribution, we develop in Section 4.2 a sequential initializing EM-based algorithm.

4.1. Modified EM Algorithm for LCGs

Let $f(q), q \in \mathbf{Q}$ be an empirical relative frequency distribution representing an unknown probability density function $\psi(q)$ such that $\int_{-\infty}^{\infty} \psi(q)dq \equiv \sum_{q=0}^{Q} f(q) = 1$. We assume that $f(q)$ is approximated by an LCG $P_{g:\mathbf{w},\mathbf{\Theta}}$ with $C_{\rm p}$ positive and $C_{\rm n}$ negative components $\varphi(q|\theta)$:

$$p_{g:\mathbf{w},\mathbf{\Theta}}(q) = \sum_{r=1}^{C_{\rm p}} w_{{\rm p},r}\varphi(q|\theta_{{\rm p},r}) - \sum_{l=1}^{C_{\rm n}} w_{{\rm n},l}\varphi(q|\theta_{{\rm n},l}) \qquad (8)$$

In line with Eq. (8), the positive weights $\mathbf{w}$ are restricted as follows:

$$\sum_{r=1}^{C_{\rm p}} w_{{\rm p},r} - \sum_{l=1}^{C_{\rm n}} w_{{\rm n},l} = 1 \qquad (9)$$

We also assume here that the numbers $C_{\rm p}$ and $C_{\rm n}$ of the components of each type are known after the initialization in Section 4.2 and do not change during the EM process. The initialization provides also the starting parameter values $\mathbf{w}^{[0]}$ and $\mathbf{\Theta}^{[0]}$.

The probability densities form a proper subset of the set of the LCGs due to the additional restriction $p_{\mathbf{w},\mathbf{\Theta}}(q) \geq 0$, which holds automatically only for probability mixtures with no negative components.

The LCG that provides a local maximum of the log-likelihood of the empirical data:

$$L(\mathbf{w}, \mathbf{\Theta}) = \sum_{q \in \mathbf{Q}} f(q) \log p_{g:\mathbf{w},\mathbf{\Theta}}(q) \qquad (10)$$

can be found using the iterative block relaxation process extending conventional EM schemes.

Let $p^{[m]}_{g:\mathbf{w},\mathbf{\Theta}}(q) = \sum_{r=1}^{C_{\rm p}} w^{[m]}_{{\rm p},r}\varphi(q|\theta^{[m]}_{{\rm p},r}) - \sum_{l=1}^{C_{\rm n}} w^{[m]}_{{\rm n},l}\varphi(q|\theta^{[m]}_{{\rm n},l})$ be the LCG at step, or iteration m. Relative contributions of each data item $q = 0, \ldots, Q$ into each positive and negative Gaussian at the step m are specified by the following respective conditional weights

$$\begin{aligned} &\pi^{[m]}_{\rm p}(r|q) = \frac{w^{[m]}_{{\rm p},r}\varphi(q|\theta^{[m]}_{{\rm p},r})}{p^{[m]}_{g:\mathbf{w},\mathbf{\Theta}}(q)}; \quad \pi_{\rm n}(l|q) = \frac{w^{[m]}_{{\rm n},l}\varphi(q|\theta^{[m]}_{{\rm n},l})}{p^{[m]}_{g:\mathbf{w},\mathbf{\Theta}}(q)} \\ &\sum_{r=1}^{C_{\rm p}} \pi^{[m]}_{\rm p}(r|q) - \sum_{l=1}^{C_{\rm n}} \pi^{[m]}_{\rm n}(l|q) = 1; \; q = 0, \ldots, Q \end{aligned} \qquad (11)$$

Using these weights, the log-likelihood of Eq. (10) can be rewritten in the equivalent form:

$$\begin{aligned} L(\mathbf{w}^{[m]}, \mathbf{\Theta}^{[m]}) &= \sum_{q=0}^{Q} f(q)[\sum_{r=1}^{C_{\rm p}} \pi^{[m]}_{\rm p}(r|q) \log p^{[m]}_{g:\mathbf{w},\mathbf{\Theta}}(q)] \\ &- \sum_{q=0}^{Q} f(q)[\sum_{l=1}^{C_{\rm n}} \pi^{[m]}_{\rm n}(l|q) \log p^{[m]}_{g:\mathbf{w},\mathbf{\Theta}}(q)] \end{aligned} \qquad (12)$$

where $\log p^{[m]}_{g:\mathbf{w},\mathbf{\Theta}}(q)$ in the first and the second brackets should be replaced with the equal terms: $\log w^{[m]}_{{\rm p},r} + \log\varphi(q|\theta^{[m]}_{{\rm p},r}) - \log\pi^{[m]}_{\rm p}(r|q)$ and $\log w^{[m]}_{{\rm n},l} + \log\varphi(q|\theta^{[m]}_{{\rm n},l}) - \log\pi^{[m]}_{\rm n}(l|q)$, respectively.

The block relaxation converging to a local maximum of the likelihood function in Eq. (12) repeats iteratively the following two steps:

1. E-step $[m+1]$: to find the parameters $\mathbf{w}^{[m+1]}$, $\mathbf{\Theta}^{[m+1]}$ by maximizing $L(\mathbf{w}, \mathbf{\Theta})$ under the fixed conditional weights of Eq. (11) for the step m, and
2. M-step $[m+1]$: to find these latter weights by maximizing $L(\mathbf{w}, \mathbf{\Theta})$ under the fixed parameters $\mathbf{w}^{[m+1]}$, $\mathbf{\Theta}^{[m+1]}$

until the changes of the log-likelihood and all the model parameters become small.

The E-step performs the conditional Lagrange maximization of the log-likelihood of Eq. (12) under the restriction of Eq. (9) to obtain the following estimates of the weights:

$$w^{[m+1]}_{{\rm p},r} = \sum_{q \in \mathbf{Q}} f(q)\pi^{[m]}_{\rm p}(r|q); \; w^{[m+1]}_{{\rm n},l} = \sum_{q \in \mathbf{Q}} f(q)\pi^{[m]}_{\rm n}(l|q)$$

Then the parameters of each Gaussian are obtained by the unconditional maximization just as in the conventional EM scheme (below "c" stands for "p" or "n", respectively):

$$\begin{aligned} \mu^{[m+1]}_{{\rm c},r} &= \frac{1}{w^{[m+1]}_{{\rm c},r}} \sum_{q \in \mathbf{Q}} q \cdot f(q)\pi^{[m]}_{\rm c}(r|q) \\ (\sigma^{[m+1]}_{{\rm c},r})^2 &= \frac{1}{w^{[m+1]}_{{\rm c},r}} \sum_{q \in \mathbf{Q}} \left(q - \mu^{[m+1]}_{{\rm c},i}\right)^2 \cdot f(q)\pi^{[m]}_{\rm c}(r|q) \end{aligned}$$

The M-step performs the conditional Lagrange maximization of the log-likelihood of Eq. (12) under the $Q+1$ restrictions of Eq. (11), and determines the conditional weights

$\pi_{\rm p}^{[m+1]}(r|q)$ and $\pi_{\rm n}^{[m+1]}(l|q)$ of Eq. (11) for all $r = 1, \ldots, C_{\rm p}$; $l = 1, \ldots, C_{\rm n}$ and $q = 0, \ldots, Q$. The modified EM-algorithm is valid until these weights are strictly positive, and the initial LCG-approximation should comply to this limitation. The iterations have to be terminated when the log-likelihood of Eq. (12) begins to decrease.

4.2. Sequential EM-Based Initialization

We assume that the number of dominant modes is equal to the given number of classes. To simplify the notation, let the empirical distribution have only two separate dominant modes representing the object and the background, respectively. The algorithm we present below is easily extended to the general case of $K > 2$ dominant modes. We assume that each dominant mode is roughly approximated with a single Gaussian and the deviations of the empirical density from the two-component dominant Gaussian mixture are described by other components of the LCG in Eq. (7). Therefore the model has the two dominant positive weights, say, $w_{{\rm p},1}$ and $w_{{\rm p},2}$ such that $w_{{\rm p},1} + w_{{\rm p},2} = 1$, and a number of "subordinate" weights of smaller absolute values such that $\sum_{r=1}^{C_{\rm p}} w_{{\rm p},r} - \sum_{l=1}^{C_{\rm n}} w_{{\rm n},l} = 0$.

The following sequential algorithm allows for estimating both the weights and parameters of the individual Gaussians in the latter LCG model, including the number of the non-dominant components.

1. Approximate a given empirical distribution $f(q)$, of gray levels in the given image, with a dominant mixture $p_2(q)$, of two Gaussians using the conventional EM-algorithm.

2. Find the deviations $\mathbf{\Delta} = [\Delta(q) = f(q) - p_2(q) : q \in \mathbf{Q}]$ between $f(q)$ and $p_2(q)$ and split them into the positive and negative parts such that $\delta(q) = \delta_{\rm p}(q) - \delta_{\rm n}(q)$:

$$\begin{array}{rcl} \mathbf{\Delta}_{\rm p} & = & [\delta_{\rm p}(q) = \max\{\delta(q), 0\} : q \in \mathbf{Q}] \\ \mathbf{\Delta}_{n} & = & [\delta_{n}(q) = \max\{-\delta(q), 0\} : q \in \mathbf{Q}] \end{array} \quad (13)$$

3. Compute the scaling factor for the deviations: $scale = \int_{-\infty}^{\infty} \delta_{\rm p}(q)dq \equiv \int_{-\infty}^{\infty} \delta_{\rm n}(q)dq$.

4. If the factor s is less than a given accuracy threshold, terminate and return the model $p_g(q) = p_2(q)$.

5. Otherwise consider the scaled-up absolute deviations $\frac{1}{scale}\mathbf{\Delta}_{\rm p}$ and $\frac{1}{scale}\mathbf{\Delta}_{\rm n}$ as two new "empirical densities" and iteratively the conventional EM-algorithm to find sizes $C_{\rm p}$ and $C_{\rm n}$ of the Gaussian mixtures, $p_p(q)$ and $p_n(q)$, respectively, approximating the scaled-up deviations. The size of each mixture corresponds to the minimum of the integral absolute error between the scaled-up absolute deviation $\mathbf{\Delta}_{\rm p}$ (or $\mathbf{\Delta}_{\rm n}$) and its model $p_p(q)$ (or $p_n(q)$). The number of the components is increasing sequentially by unit step while the error is decreasing.

6. Scale down the subordinate models $p_p(q)$ and $p_n(q)$ (i.e. scale down the weights of their components) and add the scaled model $p_p(q)$ to and subtract the scaled model $p_n(q)$ from the dominant model $p_2(q)$ in order to form the desired model $p_g(q)$ of the size $C = 2 + C_{\rm p} + C_{\rm n}$.

Since the EM algorithm converges to a local maximum of the likelihood function, it may be repeated several times with different initial parameter values for choosing the model giving the best approximation. In principle, this process can be repeated iteratively in order to approximate more and more closely the residual absolute deviations between $f(q)$ and $p_g(q)$. But because each Gaussian in the latter model impacts all the values $p(q)$, the iterations should be terminated when the approximation quality begins to decrease.

The final mixed LCG-model $p_g(q)$ has to be split into K LCG-submodels, one per class, by associating each subordinate component with a particular dominant term in such a way as to minimize the expected misclassification rate. To illustrate the association principle, let us consider the bi-modal case with the two dominant Gaussians having the mean values μ_1 and μ_2; $0 < \mu_1 < \mu_2 < Q$. Let all the subordinate components be ordered by their mean values, too. Then let those with the mean values smaller than μ_1 and greater than μ_2 relate to the first and second class, respectively. The components having the mean values in the range $[\mu_1, \mu_2]$ are associated with the classes by simple thresholding such that the means below the threshold, t, belong to the components associated with the first class. The desired threshold minimizes the classification error $e(t)$:

$$e(t) = \int_{-\infty}^{t} p_g(q|2)dq + \int_{t}^{\infty} p_g(q|1)dq. \quad (14)$$

5. Evolutionary Curve/Surface Model

The term $(\nu = \pm 1)$ in Eq.(5) specifies the direction of the front propagation. Several approaches were developed to make all fronts either contracting or expanding (see, e.g., [23]) in order to evolve in both directions and avoid overlaps between the regions.The problem can be reformulated as classification of each point at the evolving front. If the point belongs to the associated class (object), the front expands otherwise it contracts.

5.1. PDE System

The classification decision is based on Bayesian decision [24] at voxel (x, y, z) at the front. The term (ν) for each point is replaced by the function $\nu(x, y, z)$ so the velocity function is defined as:

$$F(x, y, z) = \nu(x, y, z) - \epsilon \cdot k(x, y, z). \quad (15)$$

where

$$\nu(x, y, z) = \begin{cases} -1 & \text{if } p_g(q|1) * p_s(d|1) > p_g(q|2) * p_s(d|2) \\ 1 & \text{otherwise} \end{cases} \quad (16)$$

If the voxel (x, y, z) belongs to the object, the front will expand, otherwise it will contract. Now, we put the Eq.(3) in the general form using the derivative of the Heaviside step function ($\delta_\alpha(.)$)([25]) as follows :

$$\frac{\partial \phi(x,y,z,t)}{\partial t} = \big(\epsilon \cdot k(x,y,z) - \nu(x,y,z)\big) \times \delta_{\alpha(x,y,z)}\big(\phi(x,y,z)\big)\big|\nabla\phi(x,y,z)\big| \quad (17)$$

The function $\delta_\alpha(.)$ selects the narrow band points around the front and the parameter α controls the width of the narrow band.

5.2. Registration Step

To make the proposed approach of shape-based segmentation invariant for the scaling, rotation, and translation of the object, the first step of the proposed approach is to align the image with any image from our aligned database. The deformations that we use are defined using the Free Form Deformations (FFD) as explained in [26]. The essence of FFD is to deform an object by manipulating a regular control lattice overlaid on its volumetric embedding space. One of the main advantages of the FFD technique is that it imposes implicit smoothness constraints during deformation, since it guarantees continuity at control points and continuity elsewhere. Therefore there is no need to introduce computationally expensive regularization components on the deformed shapes.

5.3. Algorithm

1. Estimate the pdf's of the object and background for the intensity gray level and shape signed distance values using the modified EM.
2. Register the image with any one of the aligned images from the database.
3. Initialize the level set function.
4. Mark the points of the narrow band.
5. For each point calculate the signed distance value (d) as the minimum Euclidean distance from V_M.
6. If $p_s(d|1) * p_g(q|1) > p_s(d|2) * p_g(q|2)$, then the front expands at this point, otherwise it contracts.
7. Go to step 4. This process is repeated until the change in the level set function is not significant.

6. Experimental Results

We illustrate the performance of the proposed techniques by applying it on different 2-D and 3-D data sets. The first example which we show is the segmentation of starfish. The segmentation separates starfish from the surrounding background so that each image has only two dominant objects ($K = 2$): the darker background and the brighter starfish. Figure 1(a) demonstrates one of the aligned starfish images from our database. Figure 1(b) shows one of the starfish images that we need to segment. Figure 1(c) shows the result of the registering the image shown in (a) to image in (b) using the algorithm proposed in [26].

(a) (b) (c)

Figure 1. (a) One of the aligned starfish images from the database, (b) Non-aligned image of starfish, (c) Results of the registration of (a) and (b)

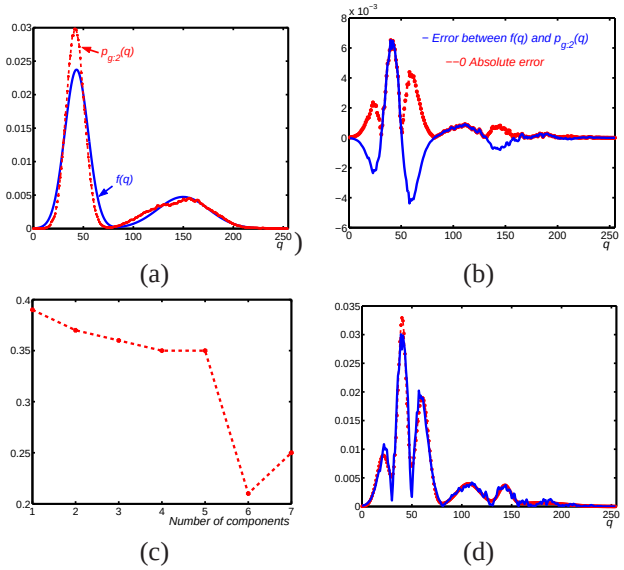

Figure 2. (a) Empirical density $f(q)$ approximated with the two dominant Gaussian components $p_{g:2}(q)$ for the image shown in Fig. 1(b), (b) Deviation and absolute deviation between $f(q)$ and $p_{g:2}(q)$, (c) Estimating the number of subordinate mixture, (d) Estimated density for the absolute deviation

Figure 2 illustrates the sequential EM-based initialization, (a) the empirical density of starfish image shown in Fig. 1(b) and the initial mixture of two Gaussians approximating the dominant modes, (b) the deviation between the empirical density $f(q)$ and the mixture of the two dominant components $p_{g:2}(q)$, (d) the estimated density of the scaled deviation using the six Gaussian components which give the minimum error between the estimated density for the deviation and the empirical deviation as shown in Fig. 2(c).

Figure 3 presents the final LCG-model and its 8 components obtained by the modified algorithm as well as the successive changes of the log-likelihood. The first 10 iterations of the refining EM-algorithm increase the log-likelihood of Eq. (12) from -4 to -2.9; then the modified EM algorithm

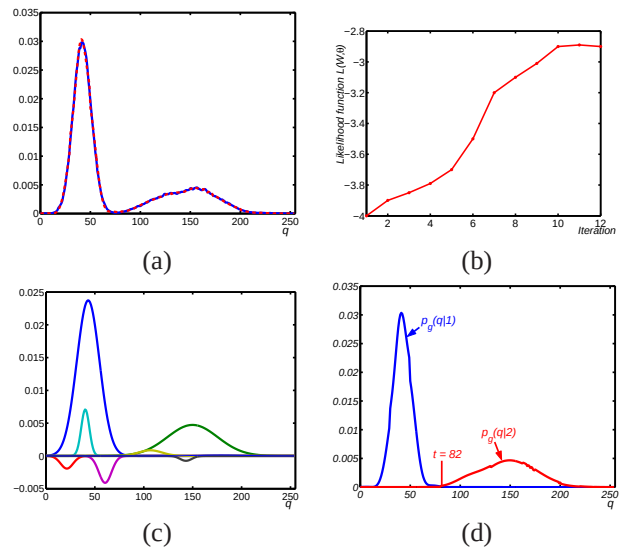

(a) (b) (c) (d)

Figure 3. (a) Final density estimation of the bi-modal distribution, (b) The dynamic changes of the log-likelihood of the modified EM algorithm, (c) All components of the final LCG, (d) The marginal density estimation for each class.

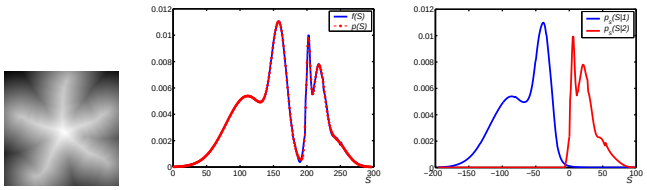

(a) (b) (c)

Figure 4. (a) Average signed distance of aligned star images, (b) Final estimated density, (c) The marginal density estimation for each class.

terminates since the log-likelihood begins to decrease. The minimum classification error of 0.00018 between the starfish and the background for the final LCG-model is obtained with the threshold $t = 82$ in Eq. (14). In this case the LCG-components 1–3 and 4–6 correspond to the starfish and the background, respectively.

Figure 4(a) shows the average signed distance of all aligned segmented starfish. We used the approach as discussed in the previous sections to estimate the marginal density that describes the distribution of signed distance inside and outside the starfish object. The results of this approach are shown in Fig. 4(b) and (c).

Figure 5 shows the result of our proposed segmentation approach with error of 0.4% with the ground truth.

In the following part, we test the proposed segmentation approach on 3D data sets to show that it can work robustly for 3D images as well. To get an accurate 3D shape model of the lateral ventricles of the brain, the 3D images were taken from 20 subjects. However, 20 data sets are not enough to get an accurate shape for the ventricles because the ventricles vibrate during the MRI or CT scans. Therefore, to cover all the shape variations of the brain ventricles for each subject,

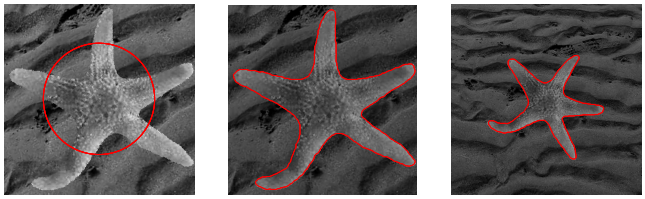

(a) (b) (c)

Figure 5. (a) The initialization of the level sets function to segment the aligned starfish shown in Fig. 1(c), (b) The segmentation of the aligned image, (c) The final segmentation of starfish after multiplying the aligned starfish image by the inverse of the transformation function (which we used in the rigid registration) with error 0.4% with the ground truth.

we performed finite element analysis on the motion of the real brain ventricles.

For finite element analysis of the ventricle shape changes, we assume the cerebrospinal fluid (CSF) inside lateral ventricles is isotropic and linear elastic. So, the linear elastic mechanical model is employed for finite element analysis. The Young's modulus of CSF is 1000 Pascals and the Poisson ratio is 0.499 ([27]). For adults, the pressure of CSF under normal conditions can range between 50 and 180 mmH_2O. The median pressure 115 mmH_2O of the CSF should be the one most people have statistically. Therefore, we apply the uniform pressure 115 mmH_2O over the surfaces of the ventricles for each subject, and perform finite element analysis to capture the variation of the ventricles. After finite element analysis, the 3D structure is re-sliced and 10 states of the ventricles are obtained resulting in 20 $subjects \times 10\ states = 200\ datasets$ for the ventricles. The four states of one subject's ventricles are shown in Fig. 6. Using the resulting 200 datasets for the ventricles, we are following our density estimation approach to estimate the density of the gray level distribution and the signed distance map inside and outside the ventricles. In this estimation, we are considering that the brain MRI consists of two classes: one class is composed of the gray matter, white matter, fat and bones; and the other class is the CSF of the brain (inside and outside the ventricles). The results of density estimation using the proposed approach are shown in Fig. 7 and the segmentation results at different signal to ratios (SNR) (obtained by adding Gaussian noise with different variance) are shown in Fig. 8.

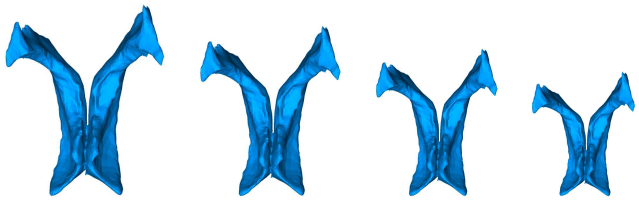

(a) (b) (c) (d)

Figure 6. The four states of the real ventricles at t = 0 sec, 0.7 sec, 0.9 sec, 1.1 sec (final) from left to right and top to bottom.

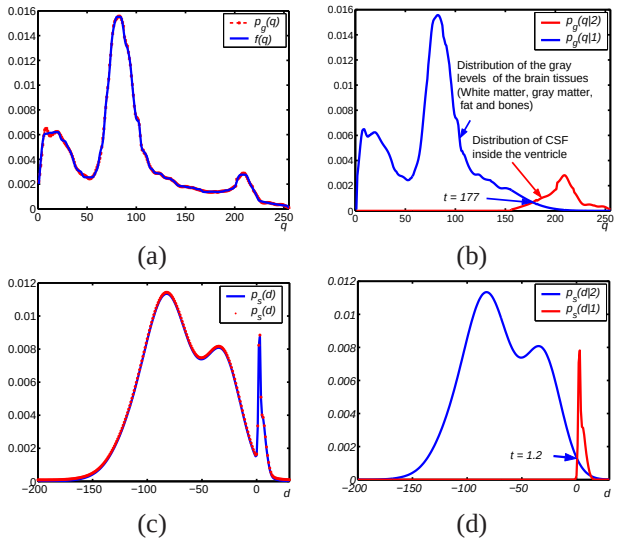

Figure 7. (a) Final density estimation for the mixed frequency gray level distribution, (b) The class model of gray level for each class, (c) Final density estimation for the sign map inside and outside the 3-D brain ventricle, (d) The final class model of signed distance map for each class.

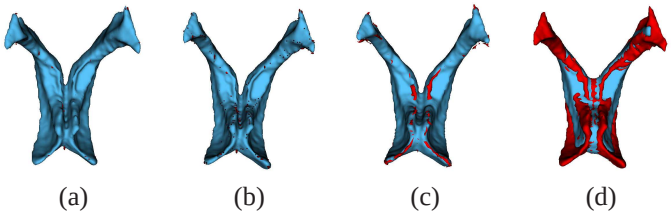

Figure 8. (a) Results of our segmentation approach at SNR = 28dB, $error = 0.23\%$ (b) SNR = 7.8dB, $error = 0.9\%$ (c) SNR = -1.9dB, $error = 4.8\%$. (d) Result of the segmentation errors using the conventional EM algorithm as a density estimator at SNR = 28dB, $error = 18.8\%$. The errors are shown in red.

The hand segmentation of the radiologists may not always be accurate because of hand shaking. Therefore, to get accurate evaluation of our proposed approach, we are using a ventricle phantom that resembles the geometrical structure of the real ventricles. To use the mould ventricle phantom, it is scanned using cone-beam CT machine so that the scans can be used for finite element simulation. Following the same procedure of the ventricle motion estimation as described above, we captured all the variations of the motion of the phantom ventricles. Figure 9 shows the four states of this ventricle phantom. The shape changes of the ventricles for the subject and the ventricle phantom are recorded in short videos that will be supplemented.

For the database that was obtained from the geometrical phantom, the inverse mapping method was used to get the same gray level distribution as of the real ventricles; the gray level distribution of which was shown in Fig. 7(b). The final step of our algorithm is to estimate the pdf that describes the signed distance map inside and outside the geometrical phantom. The results of our modified EM algorithm are shown in Fig. 10. Figure 11 shows the results of our segmentation for the geometrical phantom at different signal to noise ratios and the errors are calculated with respect to the ground truth from the phantom.

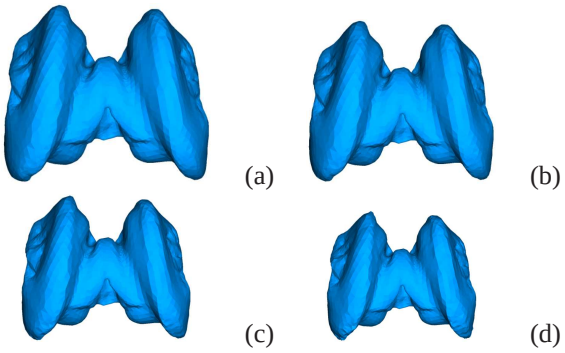

Figure 9. The four states of the phantom ventricles at t=0 sec, 0.4 sec, 0.7 sec, 1 sec (final) from left to right and top to bottom.

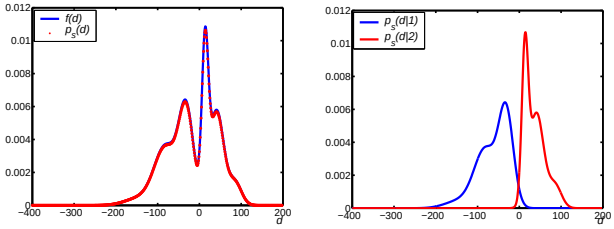

Figure 10. (a) Final density estimation for the sign map inside and outside the 3-D ventricle phantom, (b) The final class model of signed distance map for each class.

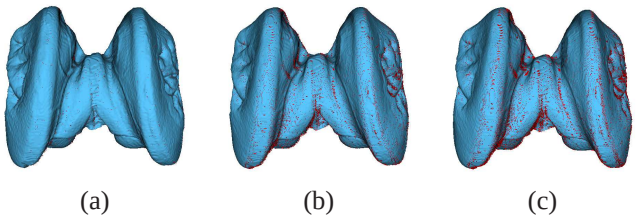

Figure 11. Segmentation using our approach at different SNR (a) $SNR = 28dB, error = 0.01\%$, (b) $SNR = 7.8dB, error = 0.8\%$ (c) $SNR = -1.9dB, error = 3.68\%$.

7. Conclusion

We have presented a segmentation approach that depends on both the intensity gray level and the shape information. Our modified EM is used to estimate the density distribution of the intensity and signed distance values. The density distributions are embedded in the PDE that controls the evolution of the level set function. We consider the registration between the average shape (2D/3D) and the object to be segmented as a basic step in our approach. Unlike the other approaches, our

segmentation does not need energy minimization avoiding the local minimum problem. Different types of images are used and the results are promising. This technique is very suitable to segment the anatomical structures that have noise and inhomogeneity problems.

This algorithm is very robust and accurate, it is invariant to translation, rotation and scaling. Therefore, the presented segmentation algorithm is not only useful for medical imaging society but also for the computer vision applications. Our future work will include the segmentation of 2D and 3D color objects.

References

[1] V. Caselles, R. Kimmel, and G. Sapiro, "Geodesic active contours," *IJCV*, 22:61–79, 1997.

[2] H-K. Zaho, T. Chan, B. Merriman, and S. Osher, "A variational level set approach to multiphase motion," *J. of Computational Physics*, 127:179–195, 1996.

[3] R. Goldenberg, R. Kimmel, E. Rivlin, and M. Rudzsky, "Cortex Segmentation: A Fast Variational Geometric Approach," *IEEE Trans. on Medical Imaging*, Vol. 21, No. 2, pp. 1544–1551, December 2002.

[4] T. Chan and L. Vese, "A multiphase level set framework for image segmentation using the mumford and shah model," *International Journal of Computer Vision*, 50(3):271-293,2002.

[5] S. Osher and N. Paragios, *Geometric Level Set Methods in Imaging, Vision, and Graphics*, Springer, 2003.

[6] D. Terzopoulos, "Regularization of inverse visual problems involving discontinuities," *IEEE Trans. on PAMI*, 8(2):413–424, 1986.

[7] X. Han, C. Xu, and J. L. Prince, "A Topology Preserving Level Set Method for Geometric Deformable Models," IEEE Transactions on PAMI, Vol. 25, No. 6, pp.755-768, June 2003.

[8] M. Leventon, "Statistical Models in Medical Image Analysis," *Ph.D. dissertation, Massachusetts Inst. Technol., Dept. Elect. Eng.*, 2000.

[9] M. Leventon, E. Grimson, and O. Faugeras, "Statistical shape influence in geodesic active contours", Proc. IEEE Conf. Computer Vision Pattern Recognition, vol. 1, pp.316-323, 2000.

[10] D. Shen and C. Davatzikos, "An Adaptive-Focus Deformable Model Using Statistical and Geometric Information," IEEE Transactions Pattern Analysis and Machine Intelligence, Vol. 22(8), 2000, pp. 906-913.

[11] A. Tsai, A. Yezzi, W. Wells, C. Tempany, D. Tucker, A. Fan, E. Grimson, and A Willsky, "A Shape-Based Approach to Curve Evolution for Segmentation of Medical Imagery", IEEE Transactions on Medical Imaging, Vol. 22, No. 2, pp.137-154, 2003.

[12] A. Tsai, W. Wells, C. Tempany, E. Grimson, and A Willsky, "Mutual Information in Coupled Multi-Shape Model for Medical Image Segmentation", Medical Image Analysis, Vol 8, No. 4, pp. 429-445, 2004.

[13] J. Yang and J. Duncan, "3D image segmentation of deformable objects with joint shape-intensity prior models using level sets", Medical Image Analysis, Vol.8, pp. 285-294, 2004.

[14] X. Huang, D. Metaxas, and T. Chen, "MetaMorphs: Deformable Shape and Texture Models," *CVPR* , pp 496–503, Washington DC., USA, June 2004.

[15] M. Rousson, N. Paragios and R. Deriche, "Implicit Active Shape Models for 3D Segmentation in MRI Imaging," *Medical Image Computing and Computer Assisted Intervention (MICCAI)*, Part 1, pp 209–216, Saint-Malo, France, September 26-29, 2004.

[16] T. Sebastin, P. Klein, and B. Kimia, "Recognition of Shapes by Editting Shock Graphs,"*In IEEE International Conference in Computer Vision*, pp 755–762, 2001.

[17] K. Siddiqi, A. Shokoufandeh, S. Dickinson, and S. Zucker, "Shocks Graphs and Shape Matching,"*International Journal of Computer Vision*, 35:13–32, 1999.

[18] S. Osher and J. Sethian, "Fronts Propagating with Curvature-Dependent Speed: Algorithms Based on the Hamilton-Jacobi Formulation,"*Journal of Computational Physics*, 79:12–49, 1988.

[19] J.A. Sethian, *Level Set Methods and Fast Marching Methods*, Combridge University Press, USA, 1999.

[20] R. Malladi, J. Sethian, and B. Vemuri, "Shape modeling with front propagation: A level set approach," *IEEE Tr. on PAMI*, 17(2):158-175, February, 1995.

[21] J. Gomes and O. Faugeras, "Reconciling distance functions and Level-Sets,", *Technical Report 3666*, INRIA, April 1999.

[22] N. Paragios and R. Deriche, "Unifying boundary and region-based information for geodesic active tracking," *CVPR*, Vol. 2, pp 300–305, Fort Collins, Colorado, June 1999.

[23] X. Zeng, L.H. Staib, R.T. Schultz, H. Tagare, L. Win, and J.S. Duncan, "A new approach to 3D sulcal ribbon finding from MR images," *MICCAI*, pp 148-157, sep. 1999.

[24] R. Duda, P. Hart, and D. Stork, "Pattern Classification," *John Wiley and Sons Inc.*, 2001.

[25] C. Samson, L. Blanc-Fraud, G. Aubert, and J. Zerubia, "Multiphase Evolution and Variational Image Classification," *Technical Report 3662*, INRIA, France, 1999.

[26] D. Rueckert, L. I. Sonoda, C. Hayes, D. L. G. Hill, M. O. Leach, and D. J. Hawkes, "Nonrigid Registration Using Free-Form Deformations: Application to Breast MR Images", *IEEE Tran. Medical Imaging*, Vol. 18, No. 8, pp. 712–721, 1999

[27] H. Takizawa, K. Sugiura, M. baba *et al.*, "Analysis of intracerebral hematoma shapes by numerical computer simulation using the finite element method," Neurol. Med. Chir. Vol. 34, pp. 65-69, 1994